Magnetism in binary and encapsulated Co-Mn clusters

A. M. Asaduzzaman[1,*] and J. A. Blackman[1,2]
[1]*Department of Physics and Astronomy, University of Leicester, Leicester LE1 7RH, United Kingdom*
[2]*Department of Physics, University of Reading, Reading RG6 6AF, United Kingdom*
(Received 14 June 2010; revised manuscript received 15 September 2010; published 11 October 2010)

Two types of Co-Mn clusters are investigated in calculations within the framework of density-functional theory. First, we consider Co clusters with 19 and 38 atoms and study the effect on the magnetization of single and double substitution by Mn atoms. In all cases the preferred configurations have the Mn aligning parallel with the Co moments resulting in an enhancement of the cluster magnetization that is consistent with experimental observation. Second, we consider Co clusters encapsulated in a shell of Mn and again examine the effect of the Mn on the Co magnetization. The Co moment at the center of the core is somewhat smaller than that of bulk Co while the net moment on the Co atoms at the interface with the Mn is significantly reduced. A reduction in the Co moment is also observed in experimental measurements. In order to match the level of reduction seen experimentally, it is necessary to postulate some degree of alloying.

DOI: 10.1103/PhysRevB.82.134417 PACS number(s): 75.75.Lf, 36.40.Cg, 75.50.Ee

I. INTRODUCTION

Magnetic transition-metal nanoclusters containing up to about 1000 atoms exhibit novel nonbulklike properties, which have been intensively investigated over the last two decades.[1,2] The interest has been further driven by the broad range of potential applications[3] of these systems in areas such as high-density recording,[4] sensors,[5] catalysis,[6] and biomedicine.[7] Due to the reduced dimensionality, properties such as the geometric structure and the magnetic moment differ significantly from those of the corresponding bulk material, of which the best-known example is the unusually high moment observed in the ferromagnetic (Fe, Co, and Ni) clusters.[8,9]

Much of the fundamental understanding of the behavior has been obtained through experiments and calculations on free-elemental nanoclusters. However additional degrees of freedom can be introduced by employing systems comprising two atomic species either in the form of a binary alloy, a core-shell cluster, or a cluster embedded in a matrix or deposited on a surface of a different material.[10] For instance, there has been interest in improving the thermal stability of ferromagnetic nanoparticles by introducing Pt to induce high anisotropy either by producing binary nanoparticles (e.g., FePt) (Ref. 4) or by depositing elemental ferromagnetic clusters on a Pt substrate.[11,12]

We consider here Co-Mn systems. Pure Co clusters, as noted, exhibit ferromagnetism with moments enhanced over the bulk values. Mn, by contrast, is antiferromagnetic in bulk.[13,14] As small clusters, however, Mn displays a net moment[15,16] due to an imbalance in the number of up and down spins (uncompensated spins). It appears that there is a tendency in the clusters for moments to order roughly ferromagnetically in planes which are coupled antiferromagnetically[17–20] (rather like γ-Mn or δ-Mn) but some refinement due to noncollinearity seems necessary for a detailed interpretation of experimental results.[20]

There have been a few studies on small bimetallic Co_nMn_m clusters.[21–23] Knickelbein[22] ($n+m=11-29$) and Yin *et al.*[23] ($n \leq 60; m \leq n/3$) have performed magnetization measurements for Co-rich clusters. A remarkable result coming from this work[23] is the observation that, for Mn concentrations up to about 25%, the net moment *increases* compared with the elemental Co cluster. The result is surprising in view of the behavior in the bulk alloys. Bulk Co-Mn alloys have been studied for many years,[24–41] with neutron-scattering experiments providing the means to determine the individual atomic moments. In the Co-rich regime, the Mn moments align antiparallel to the Co moments, and the mean moment of the alloy *decreases* monotonically[34,35] from 1.72 to 0 μ_B as the Mn concentration increases from 0% to 32%. The magnitudes of the Mn and Co moments similarly decrease. Band-structure calculations[42] on dilute Mn impurities in a Co host also predict a decrease in moment; an antiferromagnetic alignment of the impurity and host moments is marginally more stable than a ferromagnetic one.

Recently calculations have been reported specifically on the alloy clusters.[43–45] Rollmann *et al.*[45] studied icosahedral 13- and 55-atom Co clusters into which Mn impurities were introduced. They found that in most cases the moment of the cluster increased with Mn concentration in accord with the experimental observations[23] and in contrast to the bulk behavior. Calculations within a density-functional framework are used in the present paper to study Co_nMn_m clusters with different structures to the those examined by Rollmann *et al.*;[45] we examine clusters with $n+m=19$ and $n+m=38$, which as pure Co ($m=0$) are believed to have D_{5h} and O_h symmetries, respectively.[46]

The second system that we address in this paper comprises Co clusters embedded in a Mn matrix. This is motivated by recent interest in such structures as exchange coupled systems.[47,48] Co nanoparticles with a mean size of ~ 1.8 nm were produced[47,48] from a cluster source and dispersed in a Mn matrix at low volume fraction (4.7%). Exchange coupling[49] between a ferromagnet and an antiferromagnet was first reported by Meiklejohn and Bean[50] in systems of partially oxidized Co particles. Domingo *et al.*[48] find the shift of the hysteresis loop along the magnetic axis that is characteristic of exchange bias systems. In addition they find spin-glasslike behavior in the susceptibility measurements. They describe the system as a superspin glass in

which there is a random freezing of the Co particle moments coupled through the magnetic ordering of the matrix. We note that Kouvel[25] also observed shifted hysteresis loops in Co-Mn systems. In his case, the experiments were on the bulk alloy in the much studied[35–40] composition range (25–43 % Mn) between the regimes of ferromagnetic and antiferromagnetic long-range order. Domingo *et al.*[48] find that the ferromagnetic moments of the Co clusters embedded in Mn are very much smaller ($\sim$0.1 μ_B/Co atom) than the moments of similar Co particles embedded in, say, Ag. We report on electronic-structure calculations on Co particles embedded in shells of Mn atoms of varying thickness in order to investigate the effect on the Co magnetism of the interface with Mn. The calculations indicate that some degree of alloying is necessary to understand the behavior observed experimentally.

The results of the calculations on Co-Mn binary clusters are presented in Sec. III, and the Co clusters encapsulated in Mn are discussed in Sec. IV. This is preceded by a brief outline of methodology in the following section.

II. COMPUTATIONAL DETAILS

Calculations within density-functional theory (DFT) for clusters of up to 147 atoms were performed using the linear combination of atomic orbital method as implemented with the DMOL3 package[51] in parallel mode over eight processors. The atomic orbitals are obtained via a radial solution of the atomic Schrödinger equation. Double numerical basis 3*d* and 4*s* orbitals in addition to 4*p*-polarized functions are included in the valence basis set. The core orbitals are allowed to hybridize with the valence orbitals. A generalized gradient approximation (GGA) (Ref. 52) was used to represent the exchange-correlation interaction. The results appear rather insensitive to the precise choice of GGA functional, as has been noted also elsewhere.[45]

All of the calculations on the bimetallic clusters are performed using this method, as are the studies of the core-shell clusters for system sizes up to 147 atoms. Since the Co clusters of experimental interest[48] contain $\sim$280 atoms, an attempt is made to investigate larger clusters embedded in several shells of Mn by using a tight-binding (TB) methodology. The procedure, which extracts parameters from *ab initio* calculations within the linear muffin-tin orbital in the atomic sphere approximation, has been described elsewhere.[53–55] Its reliability is checked by comparison with *ab initio* calculations at the upper size limit at which such calculations can be performed, and rather good agreement is obtained.

We also perform some supercell calculations on substitutional impurities in bulk using the Vienna *ab initio* simulation package (VASP) (Refs. 56 and 57) within density-functional theory and the GGA.[58] A $2\times2\times2$ supercell with 32 atoms is considered for bulk calculations. We used projected augmented wave (PAW) (Ref. 57) potential provided in the VASP package. A $5\times5\times5$ Monkhorst-Pack *k* points is sampled in the Brillouin zone. We tested the convergence of *k* points with higher *k* points grid and obtained negligible change in the total energy.

The local magnetic moments in VASP are determined from the integration of charge in the PAW sphere for a spin-polarized calculation. The DMOL3 calculations are based on a linear combination of atomic orbitals and the moments and densities of states are obtained using a Mulliken analysis.

III. BINARY CLUSTERS

The observation[22,23] of the ferromagnetic alignment of the Mn and Co moments in alloy clusters caused some surprise because in bulk alloys at low Mn concentration the moments on the two species align antiferromagnetically.

To set the current work in context, we performed preliminary bulk calculations using the VASP package on fcc Co. We employed a 32-atom cubic supercell, and investigated the behavior when a single Mn atom was substituted for one of the Co atoms. For a lattice parameter of less than 3.57 Å we find two solutions, both with the Mn moment aligned antiparallel to the Co moments. The lowest energy solution has Mn in a high-spin state while the other at higher energy has Mn in a low-spin state. By contrast for a lattice parameter greater than 3.57 Å, there are solutions with parallel and antiparallel alignments, with the parallel one the lower in energy.

The optimized cell constant is 3.543 Å at which the moments (in μ_B) are (Co mean: 1.67 and Mn: −3.22). The optimized cell constant for the higher energy solution is 3.537 Å at which the moments are (Co mean: 1.70 and Mn: −0.43). The energy difference between these two solutions is 0.4 eV.

This lowest energy configuration is similar to that obtained by Stepanyuk *et al.*[42] for a single Mn impurity in an fcc Co host. They used a Korringa-Kohn-Rostoker Green's-function method and also found antiferromagnetic alignment of the impurity Mn moment with respect to the host Co moment. The magnitude of their Mn moment is 2.6 μ_B, which is slightly smaller than ours. They also find a metastable state. However, rather than a low moment antiferromagnetic configuration, they find a ferromagnetically aligned state with a Mn moment of 2.2 μ_B at just 0.12 eV above their lowest energy state.

It should be noted that the calculation of Stepanyuk *et al.*[42] is for a single Mn impurity whereas ours is for a low concentration ($\sim$3%) of regularly positioned Mn impurities. In view of this and the sensitivity of the behavior to lattice spacing it is not surprising that there are some differences between our calculation and that of Stepanyuk *et al.*[42] However the lowest energy state with the Mn moment antiferromagnetically aligned with the Co obtained is very similar in both calculations and is also consistent with the behavior observed in experiments on dilute bulk Co-Mn alloys.[34,35]

Increasing the lattice spacing results in a change in the lowest energy configuration from antiferromagnetic alignment of the Mn moment to ferromagnetic. It appears then that a narrowing of the 3*d*-electron band (*d* states becoming more atomiclike) favors ferromagnetic alignment of the Mn moment. This observation will be useful later in understanding behavior in finite clusters.

Now we turn to cluster systems. We consider the two clusters shown in Fig. 1, containing, respectively, 19 and 38

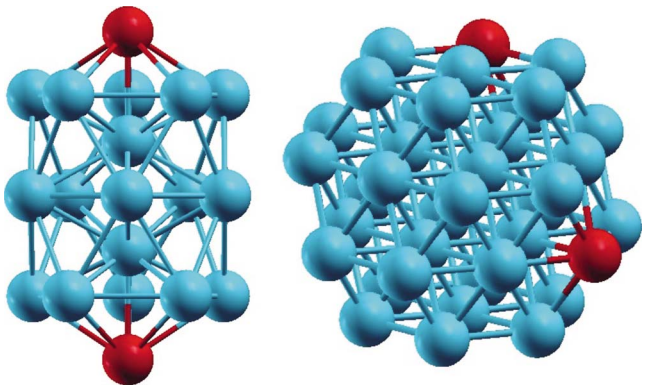

FIG. 1. (Color online) Lowest energy structures for (a) Co_{19} and (b) Co_{38}. Lowest energy impurity positions for double Mn substitution are marked by black (red) color: z1 and z4 for Co19 and (201) and ($\bar{1}$20) for Co38.

atoms. The equilibrium structure of Co_{19} is a double icosahedron and that of Co_{38} is a truncated octahedron. Lowest energy configurations were found by Zhan *et al.*[46] using a multicanonical basin hopping method and the Gupta potential. We use their coordinates as a starting point and relax the structures to their lowest energies using *ab initio* calculations. Only small changes in the coordinates occurred. Single and double Mn substitutions were then studied, relaxing the structures without any symmetry constraints. We consider only collinear spin configurations. Rollmann *et al.*[45] note that noncollinearity does not play a role in the 13-atom cluster they study and so it is unlikely to be relevant for the larger clusters that we are examining.

A. $Co_{19-n}Mn_n$

There are four inequivalent sites in the Co_{19} cluster, one internal and three on the surface of the cluster. We label atoms by their relative position along the symmetry axis starting at the top: atoms on the outer vertices (z1, z4), internal atoms on the z axis (z2, z3), central ring (r2), and outer two rings (r1, r3). For single Mn substitution this designation is sufficient because of equivalences; subsidiary labeling (for atoms in the fivefold rings) will be defined when we consider double substitution.

The results of calculations on $Co_{18}Mn_1$ clusters with substitutions at each of the four inequivalent sites are shown in Table I. We display the energy ΔE relative to the most stable configuration and the increase in magnetic moment ΔM relative to that of the Co_{19} cluster. The configuration with Mn at the outer vertex (z1 or z4) is the most stable. There is a small increase in the separation (0.08 Å) of the outer vertices compared with the Co_{19} cluster and an increase in the cluster moment of 2.2 μ_B, with the Mn moment parallel to the moments on the Co atoms. The local moments on the Mn atoms for configurations z1, r2, and r1 are 4.2–4.3 μ_B, indicating that surface Mn atoms largely retain their atomic character. A similar observation was made by Rollmann *et al.* for Mn substitution in a Co_{13} clusters.[45] The local Mn moment for z2 case is 2.2 μ_B. It was possible to obtain metastable configurations with the Mn moment antiparallel to the Co moments but these were typically ~20 meV/atom higher in energy.

TABLE I. Energy (ΔE) of the four $Co_{18}Mn_1$ structures relative to that of the most stable configuration. Also listed are the moment enhancements (ΔM) over that of the Co_{19} cluster. Configurations are labeled by the Mn substitution site (see text for site notation).

Configuration	ΔE (meV/atom)	ΔM (μ_B)
z1	0	2.2
r2	1.7	2.2
r1	2.5	2.1
z2	4.4	0.3

We now consider the substitution of a second Co atom by Mn. In this case there are 20 distinct configurations. Again parallel alignment of Mn and Co is preferred. The five lowest energy configurations are shown in Table II. The most stable configuration has the two Mn atoms occupying the outer vertices (z1, z4) of the cluster, whose separation is now 0.18 Å larger than in the Co_{19} cluster. The tendency to maximize the separation of the Mn atoms is clear from the first four entries in Table II. The pattern of high local moment on surface Mn atoms and a lower one on internal ones that was observed for the $Co_{18}Mn_1$ cluster is repeated here and manifests itself in the lower cluster moment of the (z1, z3) configuration. The most stable configuration displays an increase in moment of 4.4 μ_B. At low concentrations of Mn, therefore, the moment increase is 2.2 μ_B per substituted Mn atom, which is consistent with both experimental observation[23] and calculations[45] on Mn substitution in high symmetry Co clusters. The remaining configurations have energies ΔE ranging from 6.6 meV/atom (r1a, r3b) to 13.5 meV/atom (iv1, r1).

The densities of states projected onto the z1 site for the Co_{19} and for the $Co_{17}Mn_2$ clusters are shown in Fig. 2. The density of states (DOS) for the $Co_{18}Mn_1$ cluster is, to the

TABLE II. Energy (ΔE) of the five lowest energy $Co_{17}Mn_2$ structures relative to that of the most stable configuration, and the enhancements in moment (ΔM) compared with that of the Co_{19} cluster. Configurations are labeled by the Mn substitution sites. Where it is necessary to label atoms within a ring, we add a letter to the labeling scheme already defined. Thus r2a labels an arbitrary atom in the central ring and r2b, r2c, …, label successive atoms in the ring moving to the right with z4-z1 as the positive axis. For rings r1 and r3 we use a similar scheme with r1a and r3a labeling those at an azimuthal angle of 36° with respect to r2a.

Configuration	ΔE (meV/atom)	ΔM (μ_B)
z1, z4	0	4.4
z1, r3	2.8	4.3
z1, z3	3.1	2.5
z1, r2	3.6	4.3
r1a, r2c	4.2	4.2

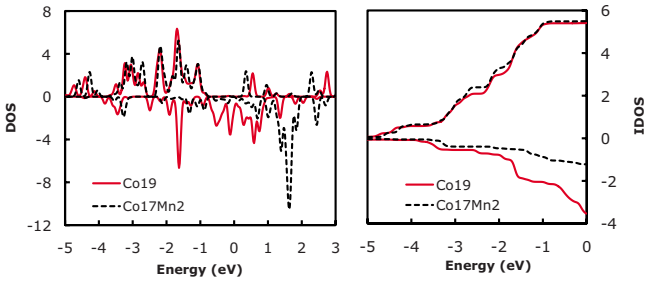

FIG. 2. (Color online) Site-projected (onto z1 site) DOS (units of eV^{-1}) and IDOS for the Co_{19} and the lowest energy $Co_{17}Mn_2$ clusters. Energy is relative to the Fermi energy.

eyes, essentially identical to that for the $Co_{17}Mn_2$ cluster. The DOS of the occupied majority-spin states is very similar for both Co in Co_{19} and Mn in $Co_{17}Mn_2$. The z1 site in this structure has only six near neighbors and so the electronic states are very atomiclike and the main effect of Mn substitution is just a change in the occupancy of the minority-spin states. This is further illustrated by the integrated DOS (IDOS) that is also plotted in Fig. 2.

The ferromagnetic alignment of the Mn impurities in the Co cluster contrasts with the antiferromagnetic alignment preferred for Mn substitution in bulk Co. This can be understood from our observations early in Sec. III that, even in bulk, ferromagnetic alignment is preferred if the lattice spacing is increased resulting in a narrowing of the 3*d* band. The band narrowing effect occurs in the cluster both through the reduced number of neighbors of the Mn defect which goes on the surface of the cluster. Also the cluster relaxes with the Mn substitution. The lowest energy configuration has the Mn atom on the z1 site. In the Co_{19} cluster the atom at the z1 position is 2.23 Å from the atom at z2 and 2.50 Å from the five atoms on ring r1. With Mn substitution, these distances are increased to 2.37 Å and 2.61 Å, respectively.

B. $Co_{38-n}Mn_n$

The Co_{38} cluster has three inequivalent sites. After relaxation, the eight atoms at the center of the hexagonal faces have coordinates [1.76,1.76,1.76] Å, the 24 atoms around the perimeters of the hexagonal faces have coordinates [3.45,1.72,0] Å, and the six atoms in reentrant positions at the square faces have coordinates [1.78,0,0] Å. For convenience we will label these sites as [1,1,1], [2,1,0], and [1,0,0], respectively.

For $Co_{37}Mn_1$, the relative energies and moment increases compared to Co_{38} are displayed in Table III. In contrast to the $Co_{18}Mn_1$ cluster, the lowest energy configuration has the Mn atom closest to the center of the cluster at a site with 12 nearest neighbors. There is a small expansion in the cluster round the Mn defect with an average increase in the distance of the neighbors of 0.03 Å. The local moment on the Mn, at 2.7 μ_B, is significantly smaller than the atomic value, which is reflected in the rather small moment enhancement (0.6 μ_B) of the cluster as a whole. The Mn atom has the same coordination (12 neighbors) as in a bulk fcc material, and so the low moment is not surprising.

TABLE III. Energy (ΔE) of the three $Co_{37}Mn_1$ structures relative to that of the most stable configuration, and enhancements in moment (ΔM) compared with that of the Co_{38} cluster. Configurations are labeled by the Mn substitution site (see text for site notation).

Configuration	ΔE (meV/atom)	ΔM (μ_B)
100	0	0.6
210	0.40	2.0
111	0.48	1.8

The relative energies and moment enhancements for a double substitution are shown in Table IV. In this case there are 28 distinct configurations. We show the lowest seven. The remaining configurations have energies ΔE ranging from 1.8 meV/atom (100, 010) to 5.7 meV/atom ($111,\bar{1}11$). The site for the lowest energy single atom substitution is not involved in the most stable double substitution configuration, Rather, the lowest energy configuration involves a pair of sites (201, $\bar{1}20$) each with the lowest coordination number (6). The separation of these sites increases by 0.14 Å compared to the Co_{38} cluster. There is a moment increase over the Co_{38} cluster of 4.1 μ_B. Double Mn substitution in both Co_{19} and Co_{38} and single Mn substitution in Co_{19} show a moment increase of slightly over 2 μ_B per substituted Mn atom while single Mn substitution in Co_{38} results in the much smaller moment increase of 0.6 μ_B.

The projected densities of states for single and double Mn substitution into Co_{38} are shown in Fig. 3 together with the corresponding Co_{38} DOS. Note that the DOS of Co_{38} shown is that projected onto the site of Mn substitution, which is different for the two plots. The majority-spin DOS is very similar for $Co_{36}Mn_2$ and Co_{38}, but less so for $Co_{37}Mn_1$ and Co_{38}, reflecting the more bulklike environment of the Mn atom in the latter case. The main contrast between the two plots is in the minority-spin states, however, and this is further illustrated in the integrated DOS plots.

TABLE IV. Energy (ΔE) of the seven lowest energy $Co_{36}Mn_2$ structures relative to that of the most stable configuration, and the enhancements in moment (ΔM) compared with that of the Co_{38} cluster. Configurations are labeled by the Mn substitution sites.

Configuration	ΔE (meV/atom)	ΔM (μ_B)
201, $\bar{1}20$	0	4.1
201, 012	0.18	4.2
201. $\bar{2}01$	0.38	4.2
201, $\bar{2}0\bar{1}$	0.45	4.1
201, $20\bar{1}$	0.70	4.0
100, $\bar{1}00$	0.97	1.1
201, $\bar{2}10$	1.06	4.0

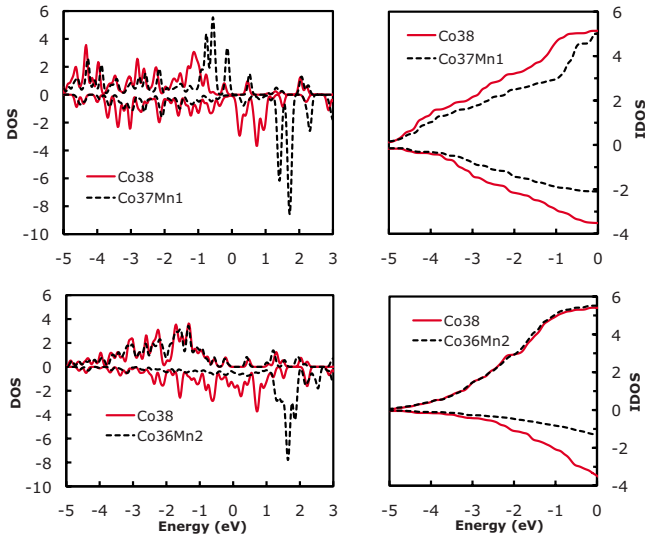

FIG. 3. (Color online) Site-projected DOS (units of eV^{-1}) and IDOS for Co_{38} and lowest energy $Co_{37}Mn_1$ and $Co_{36}Mn_2$ clusters. The projection sites are (100) for the upper panel and (201) for the lower panel. Energy is relative to the Fermi energy.

IV. ENCAPSULATED CLUSTERS

The calculations reported in this section are motivated by experimental work[47,48] on Co nanoparticles with a diameter of 1.8 nm (280 atoms) embedded in Mn. The magnetic moment on the Co was found to be minute ($\sim$0.1 μ_B/atom) in marked contrast to the behavior when similar Co nanoparticles are embedded in Ag; in that case the Co moment is close to the bulk value. It is well known[8] that isolated Co clusters exhibit a moment that is enhanced compared with the bulk value due to the reduced number of neighbors of the surface atoms while embedding Co clusters in a matrix of a noble metal results in a moment very close to that of bulk Co.[47,59] The behavior observed with Mn embedding suggests that the Mn induces some antiferromagnetic alignment within the Co cluster or possibly some quenching of the Co moment itself. That assumes that the Co nanoparticles remain pristine when embedded in Mn as they do when embedded in Ag. Some degree of alloying in the Mn case could provide an alternative explanation for the observed behavior.

Since it is not feasible to treat 280-atom clusters embedded in bulk theoretically, we investigate an allied system, namely, a core-shell structure with a Co core inside a shell of Mn. Some insight into the behavior of the embedded system can be obtained by varying the Mn shell thickness. We study fcc structures since both bulk Co and Mn have stable fcc phases with similar lattice constants. We form cuboctahedral clusters and consider first two 13-atom Co clusters within 42- and 134-atom Mn shells ($Co_{13}Mn_{42}$ and $Co_{13}Mn_{134}$), and one 55-atom Co cluster in a 92-atom Mn shell ($Co_{55}Mn_{92}$).

The results for $Co_{13}Mn_{42}$ and $Co_{13}Mn_{134}$ after geometry optimization are shown in Table V. A number of stable or metastable configurations were found using different initial conditions. The two of lowest energy, in each case, are represented in Table V. Others were of significantly higher energy than those shown. The table displays the cluster symmetries, energies relative to the lowest energy cluster, the local moments on the 13 Co sites, and the average Co moment. A conventional fcc site notation is used with (000) representing the central atom of the cluster and, of the 12 neighbors, there are four equivalent ones at (110) and eight at (101) for D_{4h} symmetry. Of course, all 12 are equivalent for O_h symmetry.

TABLE V. Local moments in μ_B on Co atoms at various sites in $Co_{13}Mn_{42}$ and $Co_{13}Mn_{134}$ clusters. Sites are indicated in conventional fcc notation (000), (110), and (101). The two lowest energy configurations of each cluster are shown and the symmetry indicated (O_h or D_{4h}). The relative energy (in meV/atom) of the two configurations of each cluster type is shown in parentheses, with the lowest energy configuration indicated as (0). The mean moments (in μ_B/atom) or the 13-atom Co core is also shown.

	$Co_{13}Mn_{42}$		$Co_{13}Mn_{134}$	
	O_h (0)	D_{4h} (1.75)	O_h (32.9)	D_{4h} (0)
000	0.90	1.36	0.89	1.08
110	0.72	−0.38	0.11	0.18
101	0.72	0.97	0.11	0.55
Mean (Co core)	0.74	0.58	0.17	0.48

It can be seen that the O_h symmetry cluster is marginally more stable than the D_{4h} one for $Co_{13}Mn_{42}$ while the D_{4h} is energetically preferred in the case of $Co_{13}Mn_{134}$. In all cases the average Co moment drops considerably below its bulk value of 1.6 μ_B. The average moment on the Co atoms interfacing the Mn is generally significantly smaller than that on the central atom with 12-fold Co coordination, although this is less marked in the O_h case of $Co_{13}Mn_{42}$. In some configurations there are examples of significant quenching of the local Co moment or some antiferromagnetic alignment. The magnitudes of the Mn moments (that are both positive and negative in sign) are in the range 3.3–4.2 μ_B for the $Co_{13}Mn_{42}$ clusters. The $Co_{13}Mn_{134}$ clusters comprise two shells of Mn atoms and the magnitude of the Mn moments on the inner shell atoms that interface with the Co are significantly reduced. This can be seen in Fig. 4.

Similar calculations were performed on a core of 55 Co atoms surrounded by a single shell of 92 Mn atoms. The results for the local moments are shown in Fig. 5. We show the results for the three configurations of lowest energies. Again solutions with O_h symmetry and D_{4h} symmetry were found, with one of the D_{4h} configurations being the most stable. The 55-atom Co core comprises a 13-atom inner core in which all atoms have 12 Co neighbors and a shell of 42 Co atoms which interface with the Mn outer shell. In all three configurations displayed in Fig. 5 the average moment on the inner core is in the range 1.2–1.4 μ_B/atom, a little less than the moment of bulk Co. For the Co atoms interfacing with the Mn, there is considerable variation in the net moment between configurations with values in the range 0.1–0.6 μ_B/atom but in all cases markedly less than the bulk moment. The mean moments for the 55-atom Co core are in the range 0.3–0.8 μ_B/atom. In summary, for the

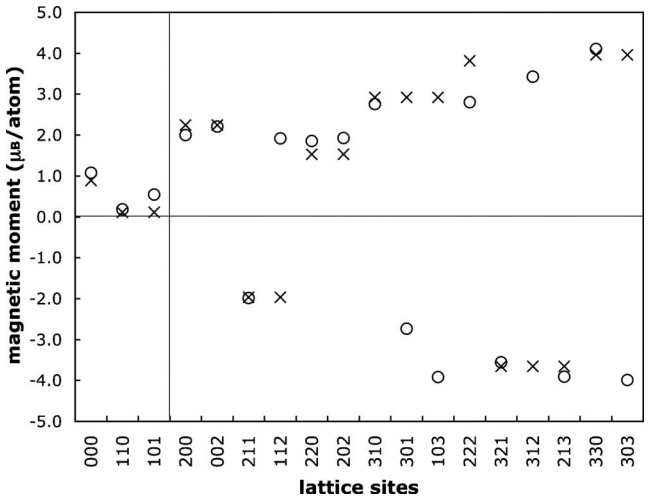

FIG. 4. Local moments (in μ_B) for sites in $Co_{13}Mn_{134}$ clusters with O_h symmetry (crosses) and D_{4h} symmetry (open circles). The vertical line indicates the position of the Co-Mn interface. The atoms in the cluster are arranged on a section of an fcc lattice with the (000) site at the center of the cluster. The lattice positions are indicated on the horizontal axis but note that these indicate the initial position of the atoms; we have allowed full geometry relaxation from those initial positions.

$Co_{55}Mn_{92}$ cluster, it appears that Co atoms that have the full fcc 12-fold coordination with other Co atoms (i.e., those in the inner core of the Co cluster) display moments somewhat reduced from the bulk value while those Co atoms at the interface with the Mn have their average moment significantly reduced. It should also be noted that the calculations include geometry relaxation but that this does not have a strong effect on the moments. The lowest energy configuration in Fig. 5 has an average Co moment of 0.79 μ_B/atom, whereas prior to relaxation the moment was little different at 0.75 μ_B/atom.

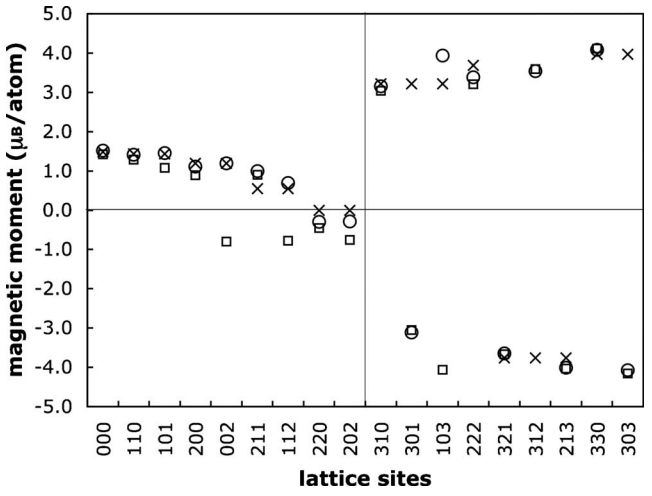

FIG. 5. Local moments (in μ_B) for atoms in a $Co_{55}Mn_{92}$ cluster. As in Fig. 4, lattice sites are shown on the horizontal axis and full geometry optimization has been performed. The local moments are shown for the three configurations with lowest energies. The one of lowest energy has D_{4h} symmetry and is indicated by open circles. The symmetries and energies (relative to that of the lowest energy configuration) of the others are D_{4h}, 7.1 meV/atom (open squares) and O_h, 15.0 meV/atom (crosses). Again the vertical line indicates the position of the Co-Mn interface.

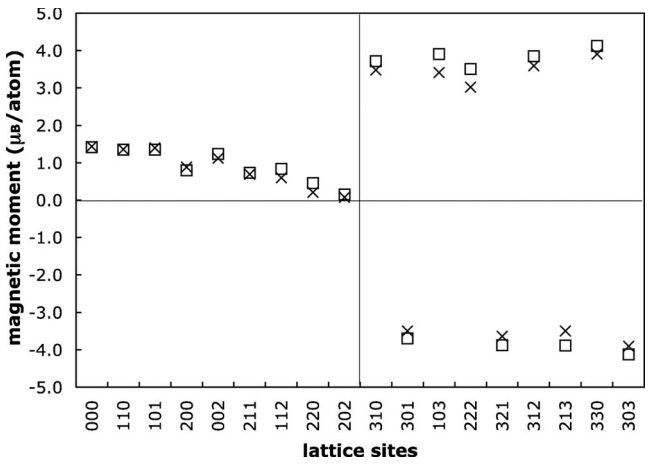

FIG. 6. Comparison of local moments (in μ_B) for atoms in an unrelaxed $Co_{55}Mn_{92}$ cluster obtained by TB (open squares) and DFT (crosses) calculations.

To facilitate the study of a wider range of core and shell sizes, we turn to the more approximate methodology of tight-binding calculations. To ensure that such calculations are consistent with the DFT results so far reported, we make a comparison of the local moments predicted by DFT and TB calculation on a $Co_{55}Mn_{92}$ cluster. We consider the moments of the lowest energy configuration illustrated in Fig. 5 and recalculate them using the TB procedure. In view of the observation that, at least for $Co_{55}Mn_{92}$, the moments are not strongly sensitive to geometry optimization, it seems an unnecessary refinement to include relaxation in the TB calculations. The results for unrelaxed geometry are shown in Fig. 6. The average Co moment is 0.81 μ_B/atom, and there is good agreement between the local moments of both Co and

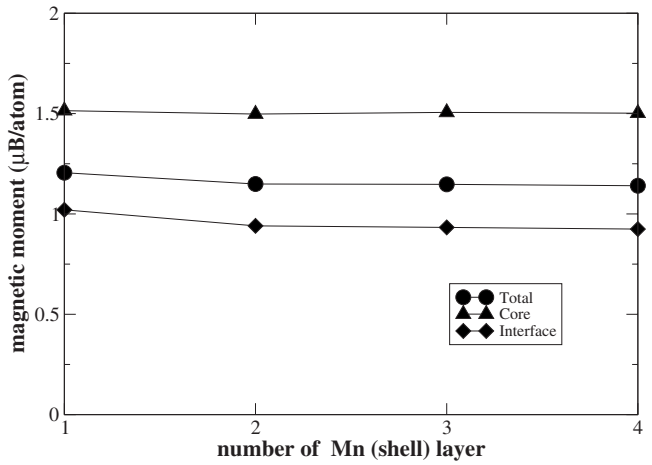

FIG. 7. TB calculated average moment on a Co_{147} cluster embedded in 1, 2, 3, and 4 shell layers of Mn. The number of Mn atoms are, respectively, 162, 252, 362, and 492.

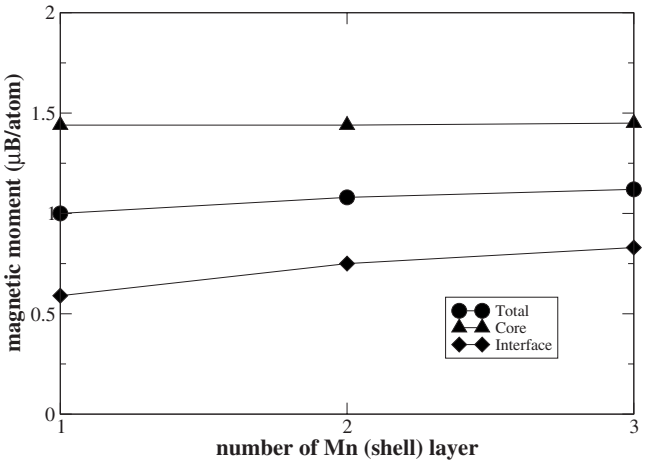

FIG. 8. TB calculated average moment on a Co_{309} cluster embedded in 1, 2, and 3 shell layers of Mn. The number of Mn atoms are, respectively, 252, 362, and 492.

Mn as calculated by both methods, providing confidence in the TB method for studying larger clusters.

We consider two Co clusters, Co_{147} and Co_{309}, which straddle the cluster sizes studied experimentally[47,48] These are embedded in shells of a range of thicknesses, and the mean moments on the Co calculated. The results are shown in Figs. 7 and 8. Besides the mean moment for the cluster as a whole, we show the mean moment on the inner core (those Co atoms that have 12 other Co atoms as neighbors) and that on the Co atoms interfacing with the Mn. The trend observed earlier is apparent. The inner core moment is just a little reduced from the bulk value while the moment on the interface atoms is significantly less ($<50\%$) than that of the bulk. For Co clusters of this size, however, the net moment is about 1 μ_B and is not strongly sensitive to the thickness of the Mn coating.

The encapsulation of a Co nanocluster within a Mn coating does depress the Co moment to significantly below its bulk value, therefore, but certainly not to the extent that is observed experimentally.[47,48] This suggests that some degree of alloying occurs with the diffusion of Co and Mn atoms between the cluster and the host.

Since we are dealing with an interface between a ferromagnetic and an antiferromagnetic component, it is worth recalling the outcome of another interface situation within a Co-Mn system. The magnetism of Mn layers deposited on a Co(001) surface has been studied as a function of layer thickness using x-ray magnetic circular dichroism and the magneto-optical Kerr effect.[60–66] The ground state of this system has been investigated theoretically by Demangeat and co-workers.[67–70] They find[69] that alloying occurs in the first layer ($Co_{0.5}Mn_{0.5}$) with both the Co and Mn atoms coupling ferromagnetically to the underlying Co. A layer of Mn on top of the interface layer orders magnetically in a $c(2\times2)$ configuration. If a further Mn layer is added, the top layer again orders in a $c(2\times2)$ configuration while the layer between it and the interface layer now orders ferromagnetically but coupled antiferromagnetically to the Co substrate. One should note that the experiments can be further complicated by oxidation.[61,65,71]

Calculations[72] of surface segregation energies show that single Mn impurities in a bulk Co host prefer a position in the interior of the host to one on the surface. This contrasts with the behavior of Ag impurities, which prefer a surface position. These calculations[72] were performed for an hcp Co surface and a single Mn (or Ag) impurity, so it would be dangerous to draw any firm conclusions about the current situation of embedded Co nanoclusters. However there do appear to be parallels. Experimental observations[47,48] of an extremely depressed Co moment when the embedding material is Mn suggest the diffusion of Mn atoms from the host into the interior of the Co cluster. By contrast Co clusters in a Ag host retain their moment.

In order to strengthen the theoretical evidence for alloying, we took one of the Co-Mn core-shell systems described above, $Co_{55}Mn_{92}$, exchanged Mn atoms in the shell with Co atoms in the core, and recalculated the energies. We recall that, in the $Co_{55}Mn_{92}$ cluster, we label atomic sites within a conventional fcc notation, with the central atom of the cluster at the (000) position. The atoms we interchange are the 24 atoms at (211) positions in the Co core with the 24 atoms at (310) positions in the Mn shell. Since the number of atoms remains fixed, we can make a direct comparison of energies with the values obtained earlier. In both calculations full geometry optimization has been employed.

As before, we obtain a number of spin configurations with either O_h or D_{4h} symmetry. Again one with D_{4h} symmetry is the state of lowest energy, and it is lower in energy by 1.5 eV than the lowest energy $Co_{55}Mn_{92}$ core-shell cluster. This provides further evidence of a tendency for Mn atoms to diffuse across the interface into the Co.

V. CONCLUSIONS

We have studied two types of Co-Mn nanostructures. We examined first Co_{19} and Co_{38} clusters that have D_{5h} and O_h symmetries, respectively, and obtained the magnetic moments on single and double substitution with Mn atoms. The general trend of an increase in cluster moment by little over 2 μ_B was observed in all but one of the cases. This is consistent with experimental observations[22,23] and with calculations on 13- and 55-atom clusters.[45] The exception to this trend is singly substituted Co_{38}, with an enhanced moment of only 0.6 μ_B and the preferred substitution site near the center of the cluster rather than one the edge as in the other cases. The parallel alignment of Mn and Co moments contrasts with the preference for antiparallel alignment that occurs in Mn substitution in bulk Co as was illustrated by a supercell calculation. It is proposed that the tendency to ferromagnetism in the clusters is associated with a narrowing of the $3d$ electron bands.

We then considered Co clusters embedded in shells of Mn. The Co moment is significantly reduced below its bulk value, with the reduction coming mainly from Co atoms interfacing with the Mn shells. For Co clusters of the size of experimental interest ($\sim$1.8 nm), the calculated mean Co moment is about 1 μ_B and is also relatively insensitive to the number of Mn shells. It is likely therefore to be a fair representation of the behavior of embedded clusters. A mo-

ment of 1 μ_B is still much larger than that observed experimentally.[47,48] Some degree of alloying is invoked as the most obvious explanation of the experimental results. Interchanging core Co atoms with shell Mn atoms leads to configurations of lower energy, and this lends support to the alloying proposal.

ACKNOWLEDGMENTS

This work was supported by the European Commission through the NANOSPIN project (Contract No. NMP4-CT-2004-013545) under the Sixth Framework Programme, Priority 3 (NMP).

*Present address: Department of Chemistry, University of Manitoba, Winnipeg, MB, Canada R3T 2N2.

[1] J. A. Alonso, Chem. Rev. **100**, 637 (2000).
[2] J. Bansmann, S. H. Baker, C. Binns, J. A. Blackman, J.-P. Bucher, J. Dorantes-Dávila, V. Dupuis, L. Favre, D. Kechrakos, A. Kleibert, K.-H. Meiwes-Broer, G. M. Pastor, A. Perez, O. Toulemonde, K. N. Trohidou, J. Tuaillon, and Y. Xie, Surf. Sci. Rep. **56**, 189 (2005).
[3] C.-H. Yu, W. Oduro, K. Tam, and E. S. C. Tsang, in *Metallic Nanoparticles*, edited by J. A. Blackman (Elsevier, Amsterdam, 2009), pp. 365–380.
[4] S. Sun, C. B. Murray, D. Weller, L. Folks, and A. Moser, Science **287**, 1989 (2000).
[5] S. H. Chung, A. Hoffmann, K. Guslienko, S. D. Bader, C. Liu, B. Kay, L. Makowski, and L. Chen, J. Appl. Phys. **97**, 10R101 (2005).
[6] S. C. Tsang, C. H. Yu, X. Gao, and K. Tam, J. Phys. Chem. B **110**, 16914 (2006).
[7] J.-W. Nam, C. S. Thaxton, and C. A. Mirkin, Science **301**, 1884 (2003).
[8] I. M. L. Billas, A. Châtelain, and W. A. de Heer, Science **265**, 1682 (1994).
[9] S. E. Apsel, J. W. Emmert, J. Deng, and L. A. Bloomfield, Phys. Rev. Lett. **76**, 1441 (1996).
[10] C. Binns and J. A. Blackman, in *Metallic Nanoparticles*, edited by J. A. Blackman (Elsevier, Amsterdam, 2009), pp. 263–277.
[11] P. Gambardella, S. Rusponi, M. Veronese, S. S. Dhesi, C. Grazioli, A. Dallmeyer, I. Cabria, R. Zeller, P. H. Dederichs, K. Kern, C. Carbone, and H. Brune, Science **300**, 1130 (2003).
[12] S. Rusponi, T. Cren, N. Weiss, M. Epple, P. Buluschek, L. Claude, and H. Brune, Nature Mater. **2**, 546 (2003).
[13] D. Hobbs, J. Hafner, and D. Spišák, Phys. Rev. B **68**, 014407 (2003).
[14] J. Hafner and D. Hobbs, Phys. Rev. B **68**, 014408 (2003).
[15] M. B. Knickelbein, Phys. Rev. Lett. **86**, 5255 (2001).
[16] M. B. Knickelbein, Phys. Rev. B **70**, 014424 (2004).
[17] T. M. Briere, M. H. F. Sluiter, V. Kumar, and Y. Kawazoe, Phys. Rev. B **66**, 064412 (2002).
[18] P. Bobadova-Parvanova, K. A. Jackson, S. Srinivas, and M. Horoi, J. Chem. Phys. **122**, 014310 (2005).
[19] M. Kabir, A. Mookerjee, and D. G. Kanhere, Phys. Rev. B **73**, 075210 (2006).
[20] Y. Xie and J. A. Blackman, Phys. Rev. B **73**, 214436 (2006).
[21] G. M. Koretsky, K. P. Kerns, G. C. Nieman, M. B. Knickelbein, and S. J. Riley, J. Phys. Chem. A **103**, 1997 (1999).
[22] M. B. Knickelbein, Phys. Rev. B **75**, 014401 (2007).
[23] S. Yin, R. Moro, X. Xu, and W. A. de Heer, Phys. Rev. Lett. **98**, 113401 (2007).
[24] J. Crangle, Philos. Mag. **2**, 659 (1957).
[25] J. S. Kouvel, J. Phys. Chem. Solids **16**, 107 (1960).
[26] G. E. Bacon and N. Cowlam, J. Phys. C **3**, 675 (1970).
[27] J. W. Cable and T. J. Hicks, Phys. Rev. B **2**, 176 (1970).
[28] M. Matsui, T. Ido, K. Sato, and K. Adachi, J. Phys. Soc. Jpn. **28**, 791 (1970).
[29] K. Adachi, K. Sato, M. Matsui, and S. Mitani, J. Phys. Soc. Jpn. **35**, 426 (1973).
[30] T. Kohara and K. Asayama, J. Phys. Soc. Jpn. **37**, 401 (1974).
[31] M. Mekata, Y. Nakashi, and T. Yamoka, J. Phys. Soc. Jpn. **37**, 1509 (1974).
[32] T. Hori, J. Phys. Soc. Jpn. **38**, 1780 (1975).
[33] D. R. Rhiger, D. Müller, and P. A. Beck, J. Magn. Magn. Mater. **15-18**, 165 (1980).
[34] J. W. Cable, Phys. Rev. B **25**, 4670 (1982).
[35] A. Z. Men'shikov, G. A. Takzeï, Y. A. Dorofeev, V. A. Kazantsev, A. K. Kostyshin, and I. I. Sych, Sov. Phys. JETP **62**, 734 (1985).
[36] M. Acet, C. John, and E. F. Wassermann, J. Appl. Phys. **70**, 6556 (1991).
[37] A. R. Wildes, S. J. Kennedy, L. D. Cussen, and T. J. Hicks, J. Phys.: Condens. Matter **4**, 8961 (1992).
[38] J. W. Cable and Y. Tsunoda, Phys. Rev. B **50**, 9200 (1994).
[39] J. W. Cable and Y. Tsunoda, J. Magn. Magn. Mater. **140-144**, 93 (1995).
[40] A. Z. Menshikov, Y. A. Dorofeev, and A. E. Teplykh, J. Phys.: Condens. Matter **8**, 5229 (1996).
[41] M. Kawakami, J. Magn. Magn. Mater. **177-181**, 1429 (1998).
[42] V. S. Stepanyuk, R. Zeller, P. H. Dederichs, and I. Mertig, Phys. Rev. B **49**, 5157 (1994).
[43] S. Ganguly, M. Kabir, S. Datta, B. Sanyal, and A. Mookerjee, Phys. Rev. B **78**, 014402 (2008).
[44] P. Wu, L.-F. Yuan, and J. Yang, J. Phys. Chem. A **112**, 12320 (2008).
[45] G. Rollmann, S. Sahoo, A. Hucht, and P. Entel, Phys. Rev. B **78**, 134404 (2008).
[46] L. Zhan, J. Z. Y. Chen, W.-K. Liu, and S. K. Lai, J. Chem. Phys. **122**, 244707 (2005).
[47] N. Domingo, A. M. Testa, D. Fiorani, C. Binns, S. Baker, and J. Tejada, J. Magn. Magn. Mater. **316**, 155 (2007).
[48] N. Domingo, D. Fiorani, A. M. Testa, C. Binns, S. Baker, and J. Tejada, J. Phys. D: Appl. Phys. **41**, 134009 (2008).
[49] J. Nogués, J. Sort, V. Langlais, V. Skumryev, S. Suriñach, J. S. Muñoz, and M. D. Baró, Phys. Rep. **422**, 65 (2005).
[50] W. H. Meiklejohn and C. P. Bean, Phys. Rev. **102**, 1413 (1956).
[51] B. Delley, J. Chem. Phys. **92**, 508 (1990).
[52] J. P. Perdew, J. A. Chevary, S. H. Vosko, K. A. Jackson, M. R. Pederson, D. J. Singh, and C. Fiolhais, Phys. Rev. B **46**, 6671 (1992).
[53] S. H. Baker, A. M. Asaduzzaman, M. Roy, S. J. Gurman, C.

Binns, J. A. Blackman, and Y. Xie, Phys. Rev. B **78**, 014422 (2008); **78**, 149901(E) (2008).
[54] Y. Xie and J. A. Blackman, J. Phys.: Condens. Matter **16**, 8589 (2004).
[55] Y. Xie and J. A. Blackman, Phys. Rev. B **74**, 054401 (2006).
[56] G. Kresse and J. Furthmüller, Phys. Rev. B **54**, 11169 (1996).
[57] G. Kresse and D. Joubert, Phys. Rev. B **59**, 1758 (1999).
[58] J. P. Perdew, K. Burke, and M. Ernzerhof, Phys. Rev. Lett. **77**, 3865 (1996).
[59] Y. Xie and J. A. Blackman, Phys. Rev. B **66**, 155417 (2002).
[60] W. L. O'Brien and B. P. Tonner, Phys. Rev. B **50**, 2963 (1994).
[61] W. L. O'Brien and B. P. Tonner, Phys. Rev. B **58**, 3191 (1998).
[62] B.-C. Choi, P. J. Bode, and J. A. C. Bland, Phys. Rev. B **58**, 5166 (1998).
[63] B.-C. Choi, P. J. Bode, and J. A. C. Bland, Phys. Rev. B **59**, 7029 (1999).
[64] S. Banerjee, W. L. O'Brien, and B. P. Tonner, J. Magn. Magn. Mater. **198-199**, 267 (1999).
[65] Y. Yonamoto, T. Yokoyama, K. Amemiya, D. Matsumura, and T. Ohta, Phys. Rev. **63**, 214406 (2001).
[66] I. Ishida and S. Morita, J. Magn. Magn. Mater. **267**, 204 (2003).
[67] B. M'Passi-Mabiala, S. Meza-Aguilar, and C. Demangeat, Phys. Rev. B **65**, 012414 (2001).
[68] S. Meza-Aguilar, O. Elmouhssine, H. Dreyssé, and C. Demangeat, Phys. Rev. B **63**, 064421 (2001).
[69] B. M'Passi-Mabiala, S. Meza-Aguilar, and C. Demangeat, Surf. Sci. **518**, 104 (2002).
[70] C. Demangeat and J. C. Parlebas, Rep. Prog. Phys. **65**, 1679 (2002).
[71] Š. Pick and C. Demangeat, Surf. Sci. **584**, 146 (2005).
[72] A. V. Ruban, H. L. Skriver, and J. K. Nørskov, Phys. Rev. B **59**, 15990 (1999).